This article was downloaded by:
On: *14 January 2011*
Access details: *Access Details: Free Access*
Publisher *Taylor & Francis*
Informa Ltd Registered in England and Wales Registered Number: 1072954 Registered office: Mortimer House, 37-41 Mortimer Street, London W1T 3JH, UK

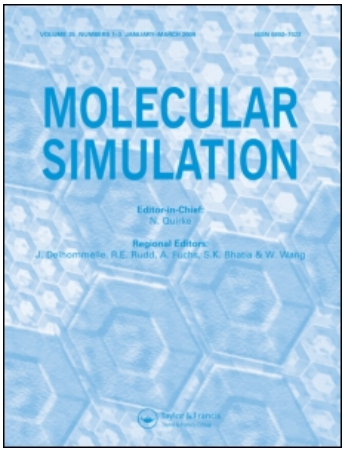

Molecular Simulation
Publication details, including instructions for authors and subscription information:
http://www.informaworld.com/smpp/title~content=t713644482

Simulations of melting of polyatomic solids and nanoparticles

Saman Alavi[a]; Donald L. Thompson[b]
[a] Steacie Institute for Molecular Sciences, National Research Council of Canada, Ottawa, Ont., Canada
[b] Department of Chemistry, University of Missouri, Columbia, MO, USA

To cite this Article Alavi, Saman and Thompson, Donald L.(2006) 'Simulations of melting of polyatomic solids and nanoparticles', Molecular Simulation, 32: 12, 999 — 1015
To link to this Article: DOI: 10.1080/08927020600823158
URL: http://dx.doi.org/10.1080/08927020600823158

PLEASE SCROLL DOWN FOR ARTICLE

Full terms and conditions of use: http://www.informaworld.com/terms-and-conditions-of-access.pdf

This article may be used for research, teaching and private study purposes. Any substantial or systematic reproduction, re-distribution, re-selling, loan or sub-licensing, systematic supply or distribution in any form to anyone is expressly forbidden.

The publisher does not give any warranty express or implied or make any representation that the contents will be complete or accurate or up to date. The accuracy of any instructions, formulae and drug doses should be independently verified with primary sources. The publisher shall not be liable for any loss, actions, claims, proceedings, demand or costs or damages whatsoever or howsoever caused arising directly or indirectly in connection with or arising out of the use of this material.

Molecular Simulation, Vol. 32, Nos. 12–13, 15 October–15 November 2006, 999–1015

Taylor & Francis
Taylor & Francis Group

Simulations of melting of polyatomic solids and nanoparticles

SAMAN ALAVI†* and DONALD L. THOMPSON‡¶

†Steacie Institute for Molecular Sciences, National Research Council of Canada, 100 Sussex Drive, Ottawa, Canada, Ont. K1A 0R6
‡Department of Chemistry, University of Missouri, Columbia, MO 65211, USA

(Received April 2006; in final form May 2006)

Molecular dynamics (MD) methods for calculating the melting point of complex molecular and ionic solids and nanoparticles are described. Various approaches for simulating melting and computing the thermodynamic melting point are discussed along with some force fields that have been used in simulations of the melting of molecular and ionic solids. The different structural, energetic and dynamical quantities used to characterize the melting transition are described. The article ends with a discussion of selected examples of melting point calculations of bulk solids and nanoparticles. Pointers on how each method can be implemented in DL_POLY are given.

Keywords: Molecular dynamics simulations; Simulations of melting; Molecular solids; DL_POLY; Melting mechanism

Downloaded At: 17:57 14 January 2011

1. Introduction

We review methods for molecular dynamics (MD) simulation of solid-to-liquid transitions. The emphasis is on methods for predicting thermodynamic melting points of polyatomic molecular and ionic solids and nanoparticles. Until recently most MD studies of melting were for atomic solids (Lennard-Jones and metals). The melting of solids composed of polyatomic molecules or ions presents a much more challenging problem. We have been interested in the development of methods for simulating melting in such materials. The simulation of melting of a solid is not as straightforward as could be assumed and involves more than running MD simulations at a number of temperatures and viewing the final outcome to determine whether the system is in an ordered solid state or a disordered liquid state. Direct heating of a periodic solid phase inevitably leads to superheating and an overestimation of the melting point. Here we review various methods for predicting melting points which avoid (or make use of) the superheating of solids and some selected studies that illustrate them. Two classes of studies for melting point determination will be outlined in Section 2. The thermodynamic method of calculating the free energies (chemical potentials) of the solid and liquid phase and methods based on the actual kinetic mechanism of melting namely homogeneous nucleation melting, surface-induced melting, or void-induced melting are discussed. Each method has advantages and associated difficulties and these will be reviewed. Methods of determining the melting point are discussed in Section 3. Realistic simulations obviously require accurate force fields, thus a discussion of MD simulations requires a discussion of force fields. These are reviewed in Section 4. A discussion of MD studies of selected polyatomic molecular and ionic solids follows in Section 4. The focus here is on methods and force fields that are readily used in DL_POLY, and throughout we will point out specifically how to implement them in simulations using DL_POLY [1].

The melting curve of a one-component system is thermodynamically defined as the set of points in the pressure–temperature phase diagram in which the molar Gibbs free energy (chemical potential) μ of the solid and liquid phases are equal. For bulk phases the thermodynamic melting curve is defined by temperatures and pressures that satisfy the condition

$$\mu_s(T, P) = \mu_l(T, P). \tag{1}$$

This constraint on the temperature and pressure means that there is only a single degree of freedom at solid–liquid equilibrium and only one of these intensive quantities of the two-phase equilibrium may be independently varied.

*Corresponding author. Email: saman.alavi@nrc-cnrc.gc.ca
¶Email: thompsondon@missouri.edu

Molecular Simulation
ISSN 0892-7022 print/ISSN 1029-0435 online © 2006 Taylor & Francis
http://www.tandf.co.uk/journals
DOI: 10.1080/08927020600823158

For a nanoparticle a solid–liquid interface phase σ is present in addition to the solid and liquid phases and the interfacial energy must be accounted for in the free energy calculations. The surface tension γ, an intensive variable, contributes to the molar free energy of the nanoparticle. At solid–liquid phase equilibrium conditions for a nanoparticle,

$$\mu_s(T, P_s) = \mu_l(T, P_l) = \mu_\sigma(T, \gamma). \tag{2}$$

Due to the surface, the hydrostatic pressures inside the solid and liquid phases are generally not equal, and there are four intensive variables that characterize the state of the system. Equation (2) imposes two constraints on the four variables and therefore at equilibrium two intensive variables may be independently varied, which means that at equilibrium pressures the solid and liquid phases in nanoparticles of different sizes (and therefore different surface tensions) can be in equilibrium at different temperatures.

2. Brief reviews of methods

We now briefly review some methods for computing melting points. We begin with the more rigorous thermodynamic integration approach and then discuss methods based on direct simulations of melting. The latter are based on simulations that correspond to the three kinetic mechanisms of melting: homogeneous nucleation, surface-induced, and defect-induced melting.

2.1 Thermodynamic integration

Two related thermodynamically rigorous pathways have been developed for calculating the melting points of solids, both of which require the calculation of the free energy of the solid and liquid phases, and involve thermodynamic integration [2] based on the Kirkwood coupling parameter method [3]. These methods have the advantage that they involve the simulation of a single phase at each stage of the calculation and thus avoid the complicating presence of interfaces in the simulation. When simulating two-phase systems care must be taken that the number of molecules in the interfacial region is not a large fraction of the total number of molecules in the simulation.

To calculate the free energy difference between states I and II, the potential energy of the system U is written as the sum of the potential energies of the two states, coupled by the parameter λ:

$$U(\lambda) = (1 - \lambda)U_{\mathrm{I}} + \lambda U_{\mathrm{II}}. \tag{3}$$

State I can represent of the system of interest and state II can be a reference state with a related potential energy function. The potential energy corresponds to that of state I for $\lambda = 0$ and state II for $\lambda = 1$. MD simulations can also be performed with potential energies for states with values of λ between 0 and 1. The derivative of the Helmholtz free energy A with respect to λ is equal to the ensemble average of the derivative of the potential energy with respect to λ: [2]

$$\left(\frac{\partial A(\lambda)}{\partial \lambda}\right)_{N,V,T} = \left\langle \frac{\partial U(\lambda)}{\partial \lambda} \right\rangle, \tag{4}$$

where the brackets represent an ensemble average. Integrating equation (4) gives the free energy difference between states I and II,

$$A(\lambda = 1) - A(\lambda = 0) = \int_0^1 \mathrm{d}\lambda \left\langle \frac{\partial U(\lambda)}{\partial \lambda} \right\rangle. \tag{5}$$

The ensemble average of the potential energy as a function of λ is first determined from MD simulations for the potential with values of λ from 0 to 1 at, say, 0.1 increments. Numerical differentiation of the ensemble average of the potential energy is then used to obtain the derivative of the free energy according to equation (4), and the result is integrated numerically with respect to λ according to equation (5) to determine the free energy difference between states I and II. The quantities involved in the evaluation of equation (5) are schematically illustrated in figure 1.

In this method for determining the melting points the absolute values of the Helmholtz free energy of the solid and liquid phases at a specified density ρ^* and temperature T^* close to the melting point are separately calculated using equation (5). Absolute Helmholtz free energies of the real solid and liquid phases are calculated with

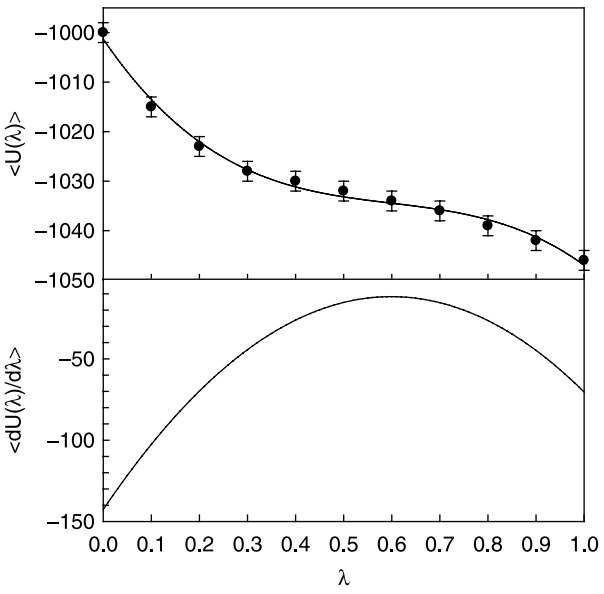

Figure 1. A schematic representation of the variation of the ensemble average potential energy $U(\lambda)$ and the derivative $\mathrm{d}U(\lambda)/\mathrm{d}\lambda$ with the switching parameter λ. The integral of the derivative plot gives the free energy of the phase according to equation (5). The $U(\lambda)$ values determined from the MD simulation have associated error bars which are schematically shown in this figure. The error bars determine the uncertainty in the slope $\mathrm{d}U(\lambda)/\mathrm{d}\lambda$ and resulting free energy.

Downloaded At: 17:57 14 January 2011

reference to standard ideal systems of known absolute free energies $A(\lambda = 1, \rho*, T*)$. The ideal reference systems for the solid and liquid phases are, respectively, the Einstein solid and the ideal gas. The density dependences of the pressures of the solid and liquid phases (i.e. the equations of state) are determined for the isotherm under consideration. Anwar *et al.* [4] have chosen the quadratic polynomial $P(\rho) = a + b\rho + c\rho^2$ as the equation of state for the condensed solid and liquid phases where a, b and c are temperature dependent adjustable parameters. More specialized equations of state such as those of Rose *et al.* [5] or Parsafar and Mason [6] for solids can also be used [4,7].

For the quadratic polynomial equation of state, the thermodynamic relation

$$A(\rho) = A^*(\rho^*) + \int_{\rho^*}^{\rho} \frac{P(\rho)}{\rho^2} \mathrm{d}\rho$$

$$= A^*(\rho^*) + \left[c(\rho - \rho^*) + b \ln \frac{\rho}{\rho^*} - a\left(\frac{1}{\rho} - \frac{1}{\rho^*}\right)\right] \quad (6)$$

allows the calculation of the Helmholtz free energies of the solid and liquid phases at density ρ from knowledge of the values at $\rho*$. Using the relation between the Gibbs free energy and the Helmholtz free energy, $G = A + P/\rho$, and the quadratic polynomial form of the equation of state, the chemical potential for each phase can be determined:

$$\mu(\rho) = \frac{A^*(\rho^*)}{N} + \left[c(2\rho - \rho^*) + b\left(\ln \frac{\rho}{\rho^*} + 1\right) + \frac{a}{\rho^*}\right]. \quad (7)$$

The melting pressure at the temperature of the chosen isotherm is determined by extrapolating chemical potentials for the solid and liquid in the $\mu - P$ plane to an intersection pressure at which the chemical potentials of the two-phases are equal, as illustrated in figure 2. It is more convenient to find the intersection in the pressure plane since the chemical potential curves are more linear in the pressure representation.

This method requires separate MD calculations for the absolute values of the Helmholtz free energy for solid and liquid phases [2,4]. Absolute Helmholtz free energies for the real phases are calculated with reference to standard ideal systems with known analytical forms for their absolute free energies. These calculations are not always straightforward for real molecular and ionic solids since there are often secondary solid–solid phase transitions and singularities in the thermodynamic pathways linking the ideal solid system to the real solid phase of interest.

Calculations of the free energies of real solids and ideal Einstein solids can be performed with potential energy functions available in the DL_POLY program. The intermolecular potential of the real solid can be any one of the types defined in the DL_POLY code and the potential for the Einstein solid involves tethering the center of mass of the molecule of interest to its equilibrium lattice site with a harmonic potential provided in DL_POLY. Calculations for values of λ between 0 and 1 for equation (3) can be straightforwardly implemented.

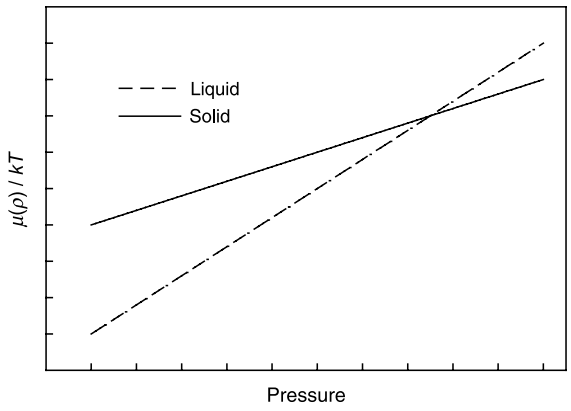

Figure 2. A schematic representation of the calculated variation of the chemical potential with pressure for the solid and liquid phases. The intersection of the two curves give the equilibrium pressure for the solid and liquid phases at the temperature of the simulation.

2.2 Thermodynamic integration via pseudo-supercritical pathways

A second free energy-based melting point determination procedure has recently been suggested that directly links the solid and liquid phases through a three-stage pseudo-supercritical pathway which avoids the discontinuous phase transition [8–9]. The free energy changes for all three of these stages can be determined by thermodynamic integration, giving the free energy change for the melting process. The melting point is a state function and does not depend on the pathway taken to link the solid and liquid states. In the first step of the procedure the intermolecular interactions in the liquid phase are gradually weakened by a factor of η from the original value U_{inter} to a nonzero value ηU_{inter} with the parameter λ according to

$$U = (1 - \lambda)U_{\mathrm{inter}} + \lambda\eta U_{\mathrm{inter}}, \quad (8)$$

and the molecules in the liquid are allowed to rearrange at the constant liquid volume. In the second step, which involves a pseudo-supercritical transformation, the volume of the simulation cell is scaled down to the solid state value and Gaussian potential wells U_{Gaussian} are turned on at locations in the simulation cell corresponding to the lattice sites of the solid phase. The molecules relax into these Gaussian wells. The residual repulsions in the ηU_{inter} term prevent more than one molecule from relaxing into the same Gaussian well. In the third step the intermolecular interactions are returned to their initial strength of U_{inter} with the volume fixed at the solid-state value and the Gaussian potential wells are turned off. The Helmholtz free energy changes can be directly determined for each stage of this pathway allowing the determination

Downloaded At: 17:57 14 January 2011

of Gibbs free energy differences between the solid and liquid phases at a given pressure and temperature. This method has been used to determine the melting point of the Lennard-Jones, NaCl and molecular solids [9–10].

The three stages of this calculation can be implemented in the DL_POLY program. The Gaussian attractive potential for the centers of mass of molecules is not directly available in the DL_POLY list of tethering potentials. For atomic species or rigid molecules, this potential can be added to the tethfrc.f subroutine in a straightforward manner.

Both free energy methods for determining the melting point are rigorous in principle, but implementing them for complex molecular and ionic solids is not straightforward. The free energy extrapolation method is often beset with singularities in the calculation of the absolute free energy of the solid state and the direct solid–liquid free energy calculation method involves the pseudo-supercritical transformation step which requires Gaussian wells to fix all the different component atoms of a flexible complex molecule in the proper lattice locations.

2.3 Direct simulations of perfect crystals: homogenous nucleation melting

In direct simulations of perfect crystals with periodic boundary conditions only homogenous nucleation melting can occur. This mechanism is analogous to homogeneously nucleated condensation of gases. The free energy barrier to the formation of a solid–liquid interface in perfect crystalline solids leads to hysteresis and superheating of the solid prior to melting. According to the theory of homogeneous nucleation melting [11] the free energy barrier β to nucleation in the solid state is given by,

$$\beta = \frac{16\pi\sigma_{\mathrm{sl}}^3}{3\Delta H_m^2 k T_{\mathrm{m}}}; \tag{9}$$

where σ_{sl} is the solid–liquid surface tension, ΔH_{m} is the enthalpy of fusion, and T_{m} is the equilibrium melting temperature. This free energy barrier causes superheating of perfect solids in simulations of melting and a supercooling of liquids in simulations of freezing. The hysteresis effects for constant-pressure MD simulations of a solid and a liquid are schematically illustrated in figure 3. The density of a periodic simulation cell is plotted as a function of the temperature for heating (open symbols) and cooling (filled symbols) simulations. In a heating simulation of a solid there is a sudden drop in density upon melting at T_+ and a cooling simulation of a liquid there is a jump in the density at T_- due to fusion. Studies of metallic and some molecular solids show that the thermodynamic melting point can be estimated from the magnitudes of superheating, T_+, and supercooling, T_-, temperatures: [11,12]

$$T_{\mathrm{m}} = T_+ + T_- - \sqrt{T_+ T_-}. \tag{10}$$

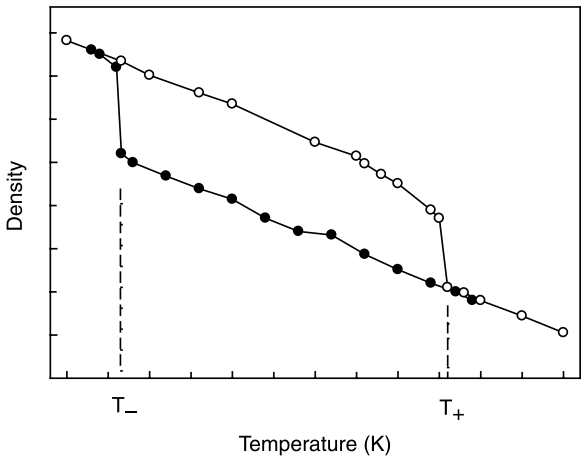

Figure 3. This illustrates the MD results of the hysteresis loop due to the superheating of the solid and supercooling of the liquid. The melting point can be determined from the superheating and supercooling temperatures, T_- and T_+, respectively, using equation (10).

The superheating temperature can usually be determined with good accuracy from simulations, but for complex molecular systems the supercooling temperature is difficult to observe because in simulations the liquid often undergoes a transition to an amorphous rather than a crystalline solid. The liquid–solid and liquid–glass transitions are characterized by a decrease in the diffusion coefficient of the molecules to values in the order of $10^{-11}\,\mathrm{m}^2/\mathrm{s}$, values typical of solids. It has empirically been found that the glass temperature T_{g} can be substituted for the supercooling temperature T_- in equation (10) [12]. A further complication can arise since the perfect crystals of some solids can be superheated to very high temperatures without melting; see the discussion of 1-*n*-propyl-4-amino-1,2,4-triazolium bromide [patr] [Br] [13] in Section 5. The method is obviously not applicable in such cases.

Two methods have been used for gradually increasing the temperature of a simulation supercell to observe melting. For continuous heating/cooling the dlpoly.f subroutine of DL_POLY can be modified to change the temperature of the system by ΔT at specified time intervals during run time. The system is partially equilibrated between temperature changes. Alternatively, a script can be written which automatically restarts a new calculation with incremental heating/cooling at a temperature $T + \Delta T$ after completing an equilibration simulation at temperature T. This latter method allows for better equilibration of the simulation at each temperature and slower heating compared to the case where the temperature continuously changed within a single MD run. Zheng *et al.* [12] have used the incremental method to calculate the melting point of nitromethane (NM) using equation (10). The temperatures of the system were changed at rates of 10^9–$10^{11}\,\mathrm{K/s}$, which are very high compared to experimental heating rates, but resulted in a value of the melting point in good agreement with experiment.

Downloaded At: 17:57 14 January 2011

Downloaded At: 17:57 14 January 2011

2.4 Simulations of solid and liquid phases in contact

In simulations of coexisting solid and liquid in contact [14] the free energy of formation of the solid–liquid interface has already been provided to the system. A sample initial configuration for a two-phase simulation for a monatomic model system is shown in figure 4. There is a contact surface in the middle of the simulation cell and due to periodic boundary conditions, there will be a second contact surface between the solid and liquid at the edges of the simulation cell.

Roughly equal amounts of solid and liquid phases are equilibrated separately in NPT simulations at a temperature above the melting point. The simulation cell for the two-phase simulation merges the final REVCON files of these two runs in such as way that the z-coordinates of one of the files are shifted on top of the other, with equal cross sections in the xy-plane (the solid–liquid boundary plane). The two phases are partially equilibrated with an NVT simulation to allow the molecules at the contact surface to relax to more stable positions. The two-phase system is then subject to a NVE simulation [14–15]. As the simulation progresses some of the solid at the interface will melt. This removes kinetic energy, lowering the temperature. Melting continues until the equilibrium is established and the temperature of the two-phase system converges to the true solid–liquid equilibrium value at the simulation pressure. This method has been used to determine the melting points for atomic and molecular solids [15–17]. It requires long simulation times and large simulation supercells to obtain converged values of the melting temperature. A fairly large number of molecules (between 880 and 16,000 molecules) [15–17] must be used to minimize the surface effects on the thermodynamics of the melting.

2.5 Defect-induced melting

The free energy barrier to the formation of a solid–liquid interface can be eliminated by introducing molecular Schottky defects [18] or voids into a simulation cell [15–17]. The melting point can be determined by performing NPT simulations as functions of temperature (varied either continuously or incrementally) and the number of voids [15–17,19]. As the system equilibrates the structure of the solid in the vicinity of the voids collapses and local pockets of liquid-like structure form. The voids effectively lead to the formation of solid–liquid interfaces, which lowers, and for sufficient number of voids, eliminates, the free energy barrier for the conversion of the solid to the liquid. Increasing the number of voids in a crystal results in a decrease of the calculated melting temperature until a sufficient number of voids have been introduced to eliminate the free energy barrier, at which point the computed melting temperature levels off in what is called the plateau region, as illustrated in figure 5. The plateau region extends over a limited range of the number of voids, usually about 5–10% of the total number of molecules (or ion pairs) in the simulation supercell. Studies show that the distribution of voids in the simulation cell does not affect the melting point predictions [15]. The void-induced melting method allows the use of three-dimensional periodic boundary conditions and is more convenient for high-pressure simulations than other methods that introduce free surfaces or grain boundaries [17]. After the introduction of voids, a sufficient amount of the solid must remain in the simulation supercell to maintain the integrity of the crystal structure. If too many voids are introduced, the solid becomes mechanically unstable and collapses without a discontinuous solid-to-liquid phase transition [16,20–21]. The voids can be

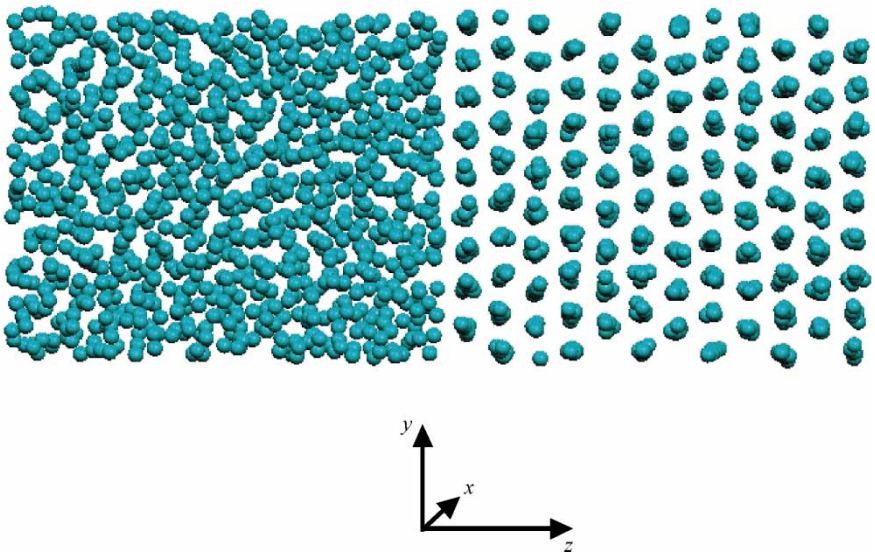

Figure 4. An illustration of an initial configuration for two-phase solid–liquid NVE simulation. Shown is a FCC atomic solid in contact with its liquid. Also, shown is a reference frame used in the discussions in the text.

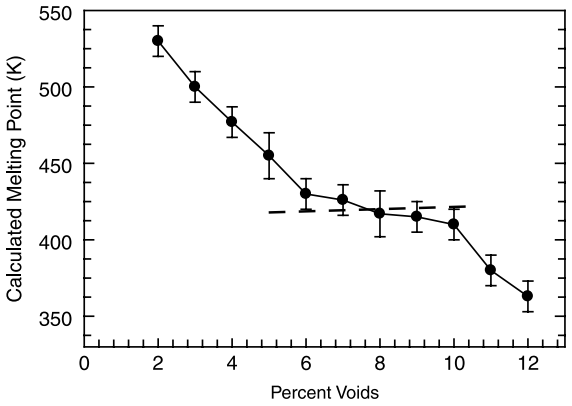

Figure 5. The calculated melting point as a function of the percent of voids into the simulation supercell. The temperature corresponding to the plateau (illustrated by the dashed line) is taken to be the thermodynamic melting point.

introduced by removing molecules or adjacent ion-pairs in the case of ionic solids from the CONFIG or equilibrated REVCON file.

2.6 *Melting of nanoparticles*

Melting of nanoparticles is a first-order transition, although orientational disordering of complex molecules in a nanoparticle, which gives rise to second-order phase transitions has also been observed [22]. The melting of nanoparticles of different sizes can be directly calculated by placing annealed nanoparticles in vacuum and performing NVT simulations over a range of temperatures. Because of the solid–vacuum interface there is no free energy barrier to melting in nanoparticle simulations. Thus, the simulation yields the thermodynamic melting point as a result of surface-induced melting.

Initial conditions for nanoparticles of any composition can be constructed by constructing a CONFIG file for a block of the solid without periodic boundary conditions. By using a replica of the solid-state unit cell, we guarantee that the initial structure used in the simulation of the nanoparticle has a zero net dipole moment. The solid block is positioned in a simulation cell surrounded by vacuum. It is then annealed in a NVT simulation. This usually leads to a relatively stable nanoparticle structure close to the global minimum potential energy after a few cycles of heating and cooling. The annealing process can be particularly important for nanoparticles of large molecules or ions, since the strong interactions can trap the structure in a configuration far from the most stable structure. In nanoparticle simulations the electrostatic forces are calculated directly; i.e. Ewald summations of electrostatic point charges are not used.

The extra degree of freedom for the solid–liquid equilibrium in a nanoparticle results in the size dependence of the melting point and different thermodynamic models have been proposed to quantitatively describe the radius r (or mass) dependence of the melting point [23–27]. Macroscopic thermodynamics-based surface premelting models [23–25] can be used to describe the size dependence of the melting point for nanoparticles with radii of about 50 Å or larger. In this size regime melting first occurs in a surface overlayer of the nanoparticles of thickness t_0 and progresses inward as the temperature is increased. The solid core and the liquid outer shell can be in equilibrium over a range of temperatures. According to the analysis of Hanszen [23] the melting point $T_{\mathrm{m,n}}$ of a nanoparticle of radius r is related to the melting point of the bulk phase $T_{\mathrm{m,b}}$ by

$$T_{\mathrm{m,b}} - T_{\mathrm{m,n}} = \frac{2T_{\mathrm{m,b}}}{\Delta H_{\mathrm{m},b}}\left[\frac{\sigma_{\mathrm{sl}}}{\rho_{\mathrm{s}}(r - t_0)} + \left(\frac{\sigma_{\mathrm{lv}}}{r} + \frac{\Delta P}{2}\right)\left(\frac{1}{\rho_{\mathrm{s}}} - \frac{1}{\rho_{\mathrm{l}}}\right)\right]; \tag{11}$$

where $\Delta H_{\mathrm{m,\ b}}$ is the enthalpy of fusion, σ_{sl} and σ_{lv} are, respectively, the solid–liquid and liquid–vapor surface tensions, ρ_{s} and ρ_{l} are, respectively, the solid and liquid density, and ΔP is the difference in the vapor pressure at the surface of a liquid droplet of radius r and that of the flat bulk surface (radius $r = \infty$). The quantities in equation (11) can be calculated or determined experimentally. The most difficult quantities to determine are the surface tensions. Theoretical methods based on thermodynamic integration [28] and homogeneous nucleation theory [29] can be used to calculate the surface tension of model solids and metals. The size dependence of the melting point predicted by equation (11) has been experimentally verified for metallic nanoparticles [24].

For nanoparticles with radii smaller than ≈ 50 Å the dynamic coexistence melting mechanism may be observed. In this size regime over certain temperature ranges the system is bistable and fluctuates between solid and liquid states; [30] the free energy surface has two minima corresponding to the solid and liquid states of the nanoparticle. The ratio of the two states in an ensemble of nanoparticles is given by an equilibrium constant $K =$ [solid]/[liquid] $= \exp(-\Delta G/kT)$, where ΔG is the free energy difference between the solid and liquid forms of the nanoparticle. This equilibrium constant can be estimated from the fraction of time during a simulation that a particular nanoparticle spends in the solid and liquid states.

3. Characterizing the melting point

Melting is a first-order phase transition that is characterized by discontinuous first derivatives of the Gibbs free energy (i.e. entropy and volume), while maintaining constant temperature and pressure. At the melting pressure, P_{m}, and temperature, T_{m}, of solid–liquid equilibrium,

$$\left(\frac{\partial G_{\mathrm{s}}}{\partial T}\right)_{Pm} = -S_{\mathrm{s}} \neq -S_{\mathrm{l}} = \left(\frac{\partial G_l}{\partial T}\right)_{Pm}, \tag{12}$$

Downloaded At: 17:57 14 January 2011

Downloaded At: 17:57 14 January 2011

and

$$\left(\frac{\partial G_s}{\partial P}\right)_{Tm} = V_s \neq V_l = \left(\frac{\partial G_l}{\partial P}\right)_{Tm} \tag{13}$$

where the subscripts s and l indicate solid and liquid properties, respectively. At the melting transition there is a sudden shift in the arrangement of the molecules from the solid to the liquid state with a corresponding sudden change in energy, entropy, heat capacity, density and other extensive properties. These properties can be used to determine the melting temperature. Structural properties, e.g. radial distribution functions (RDF) and root-mean-square displacement can be used to ascertain that the transition is complete. Properties such as the Lindemann parameter (i.e. average interatomic distances), the diffusion coefficient, order parameters, and dipole–dipole correlations can also be used to determine the melting point.

The volume and density are straightforward to compute. The simulation cell volume at each temperature can be read from the DL_POLY OUTPUT or STATIS file and plotted using the DL_POLY GUI. The average volume should be stable over the equilibration period of the simulation and the volume fluctuations should be less than the 10%, which is the typically observed difference in a solid to a liquid. The magnitude of the volume fluctuations in a NPT simulation is influenced by the barostat and thermostat relaxation times. In the following we give the equations for some of the other properties commonly used to determine melting points.

The melting transition can be observed in volume versus time versus time plots at temperatures above the melting point. The change in the simulation cell volume over the duration of a simulation of a perfect crystal of the room-temperature ionic liquid ethyl-methylimidazolium hexafluorophostate, [emim] [PF_6], is shown in figure 6. The melting occurs in the isothermal trajectories at $T = 550$ K and higher.

3.1 Structural characterizations

Structural characterizations should be used with other criteria since discontinuous changes in structure are a necessary, but not a sufficient indicator of melting—they may also indicate a solid–solid or solid–glass phase change. Large qualitative changes in the structure of the RDF and changes in the value of the order parameters occur for second-order order–disorder transitions (such as solid to glass transitions), thus the nature of the transition causing the structural changes must be verified with other criteria.

The translational order parameter, $\rho(\mathbf{k})$, is defined as [31,32]

$$\rho(\mathbf{k}) = \frac{1}{N}\sum_{i=1}^{N} \cos(\mathbf{k}\mathbf{r}_i), \tag{14}$$

where $\mathbf{k}$ is the reciprocal lattice vector of the initial lattice, and $\mathbf{r}_i$ is the position of the center of mass of molecule i. Other variations for the translational order parameter have been used to characterize melting in the special case of orthorhombic simulation cells [12,15,33]. The translational order parameters are related to the Fourier transform of the RDF for the center of mass of molecules in the simulation cell.

Orientational order parameters can be defined as [32]

$$\langle \cos\theta_i \rangle = \frac{1}{N}\sum_{i=1}^{N} \mathbf{u}_{\mu,i}\mathbf{u}^0_{\mu,i}. \tag{15}$$

where $\mathbf{u}_{\mu,i}$ is a unit vector representing the direction of the molecular dipole moment or some other specific internal

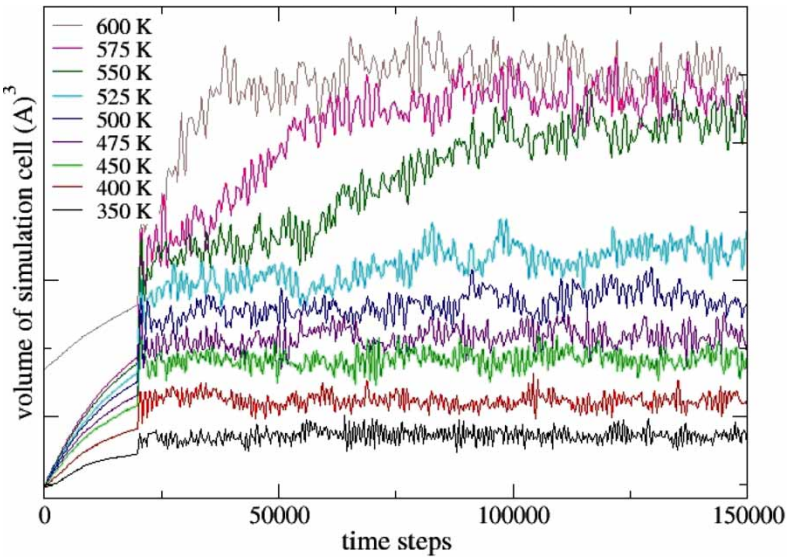

Figure 6. The volume of a [emim] [PF_6] simulation cell as a function of time (each time step = 2 fs) for temperatures over the range 350–600 K. Due to thermal expansion, the volume of the solid increases as the temperature is raised. When melting occurs there is a discontinuous jump in the volume as shown here between 525 and 550 K isotherms. The lowest temperature for which the volume jump is observed is taken to be melting point. The first 20,000 time steps of the simulation are for equilibration.

direction in the molecule (such as a unit vector pointing from atom A to B) and $\mathbf{u}^0_{\mu,i}$ is the same vector in a perfect crystal lattice. An orientational order parameter can also be based on the relative orientations of neighboring molecules i and j: [19(b),34]

$$\langle \cos \theta_{ij} \rangle = \frac{2}{N(N-1)} \sum_{i=1}^{N-1} \sum_{j=i+1}^{N} \mathbf{u}_{\mu,i} \mathbf{u}_{\mu,i}. \qquad (16)$$

Orientational order parameters are most useful for identifying solid-state phase transitions and melting in nanoparticles of dipolar molecules.

The RDF, $g(r)$, defined as

$$g(r) = \frac{1}{\rho N} \left\langle \sum_i \sum_j \delta[r - \mathbf{r}_{ij}] \right\rangle \qquad (17)$$

gives the spatial distribution of molecules i with respect to molecules j. The RDF for a crystal has sharp peaks that extend to large separations between atoms i and j, but these peaks and the spatial correlations they represent are destroyed upon melting. The large changes in the RDF upon melting can be used to determine the melting temperature.

3.2 Energy characterizations

The intermolecular energy (sum of intramolecular, van der Waals, and electrostatic energies) changes discontinuously at the melting point. If the energies of the phases are calculated with sufficient accuracy during the simulations, the heat capacity can be determined from them. The heat capacity becomes sharply peaked at the melting point and may give an easier means of identifying the melting point than the energy. However, the heat capacity is very sensitive to fluctuations in the energy.

Energy versus time plots can also be used to identify bistability in an equilibrium between the liquid and solid phases in nanoparticles, [35] as illustrated in figure 7. The isotherm at 440 K jumps between higher and lower values of the potential energy and is bistable. The 325 and 600 K isotherms on the other hand are stable and represent the solid and liquid phases, respectively. The bistable range of temperatures for this specific nanoparticle is shown in figure 7(b). The upper and lower limits of the bistable region at different temperatures are determined from the kind of data shown in figure 7(a).

3.3 Dynamic characterizations

Melting can also be identified by calculating the root-mean-square displacements (RMS) of the center-of-mass of molecules in the system,

$$\Delta |r(t)|^2 = \frac{1}{N} \left\langle \sum_{i=1}^{N} |\mathbf{r}_i(t) - \mathbf{r}_i(0)|^2 \right\rangle, \qquad (18)$$

where $\mathbf{r}_i(t)$ is the location of the center-of-mass of molecule i at time t and the brackets $\langle\,\rangle$ indicate an ensemble average. The molecules in the liquid phase have translational freedom. Thus at long times the center-of-mass RMS displacements of the molecules in a liquid will vary linearly with time, distinguishing the liquid state. The RMS displacements can be obtained from the DL_POLY GUI.

The diffusion coefficient, D, and the Lindemann index, δ, are related to the RMS displacement and can be used to characterize a melting transition. The diffusion coefficient can also be obtained from the time-correlation function of the center of mass velocities $\mathbf{v}_i$ for the molecules or ions:

$$D_i = \frac{1}{3} \int_0^\infty \langle \mathbf{v}_i(t) \mathbf{v}_i(0) \rangle \mathrm{d}t. \qquad (19)$$

The typical diffusion coefficient in a solid is on the order of $10^{-11}\,\mathrm{m}^2/\mathrm{s}$, which increases by an order of magnitude upon melting.

The Lindemann index is defined as

$$\delta = \frac{2}{N(N-1)} \sum_{i<j} \frac{\sqrt{\left\langle r_{ij}^2 \right\rangle_t - \left\langle r_{ij} \right\rangle_t^2}}{\left\langle r_{ij} \right\rangle_t}. \qquad (20)$$

It can be used to characterize the melting transition in bulk solids and nanoparticles [36]. Unlike the root-mean-square displacement, which depends on the absolute displacement of atoms, $\mathbf{r}_i(t)$, and thus is affected by the center-of-mass translational or rotational motion (particularly for nanoparticles), the Lindemann index is calculated directly from the magnitude of the separation of two molecules, r_{ij}, in the simulation without further adjustment. The Lindemann index can be determined from the data given in the HISTORY file.

Most of the properties that are used to determine the melting point and to characterize the state of the system can be directly obtained from the DL_POLY OUTPUT, RDFDAT or STATIS files; others require writing code that manipulates the coordinate, velocity, and force data from the HISTORY file. It can be possible to write subroutines for the DL_POLY code that would compute these quantities during the runs.

4. Force fields

There are several standard force field packages that have been formulated and validated for several classes of compounds for equilibrium gas-, liquid-, solution- or solid-phase properties. These general force fields provide a reasonable starting point for the development of force fields to describe melting; however, none of them are specifically parameterized to reproduce experimental melting points. The studies to date, which must be viewed as limited and preliminary, indicate that these general force fields can be used to accurately predict the melting points of ionic solids and molecular solids of compounds

Downloaded At: 17:57 14 January 2011

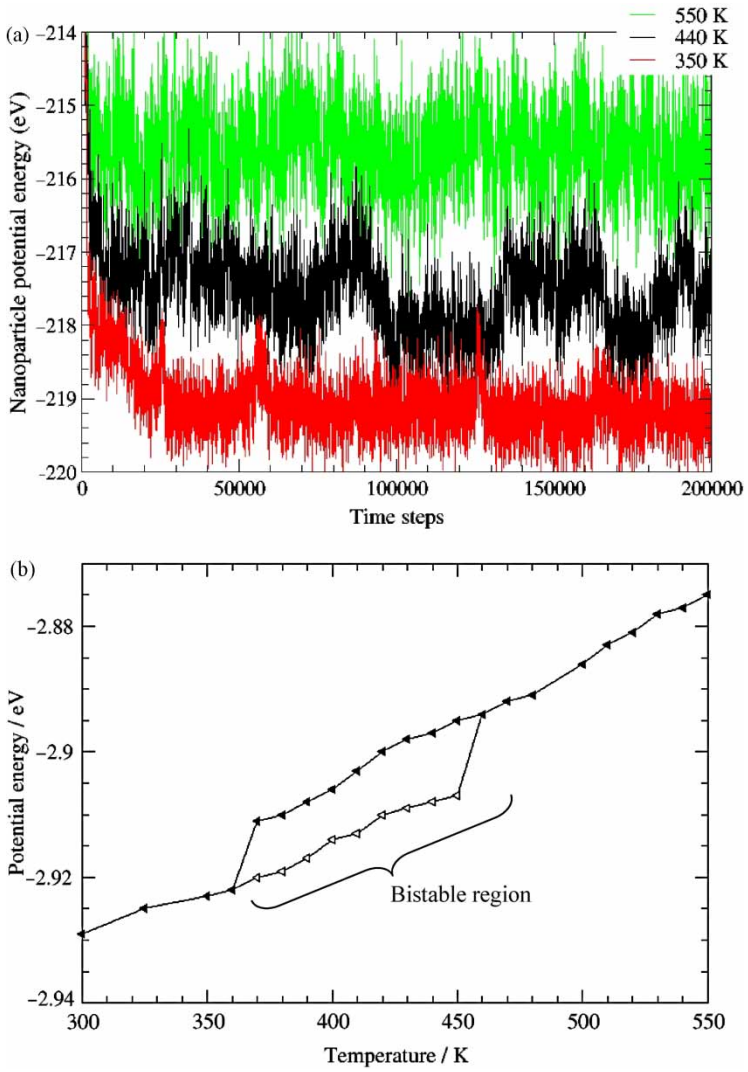

Figure 7. (a) The variation of the potential energy at three temperatures as a function of time for an aluminum nanoparticle with 75 atoms. The first 25,000 time steps of these trajectories are for equilibration and are not considered when determining the state of the nanoparticle. The jumps between high-density solid phase and low-density liquid phase in the 440 K trajectory shows the presence of bistability for this nanoparticle. (b) The potential energy as a function the temperature for the nanoparticle. In the range of 360–460 K, the isotherms are bistable and the upper (liquid) and lower (solid) limits of the potential energy are shown in this range. These limits are determined from energy—time plots shown in part (a).

of the classes used in their parameterization, but that the force fields must be modified to accurately describe solids of molecules containing functional groups not considered in their formulation, e.g. nitro and nitramine groups. More studies are needed to determine which features of a force field are most important for accurate descriptions of phase transitions. The efforts to develop better force fields for simulating melting would be facilitated by having a better understanding of the atomic-level details of melting mechanisms for polyatomic materials.

The force fields are generally written as sums of intra- and inter-molecular potentials, e.g.

$$V_{\text{total}} = \left\{ \sum_{\text{bonds}} V_{\text{b}} + \sum_{\text{angles}} V_{\text{a}} + \sum_{\text{dihedrals}} V_{\text{d}} \right\} + V_C + V_{\text{vdW}}. \tag{21}$$

The bond stretching potentials V_{b} are usually represented by harmonic or Morse functions, the angle bending potentials V_{a} by harmonic functions, and the dihedral potentials V_{d} by a three-term cosine series or $\cos(n\tau)$ form. The Coulombic potential V_C is usually expressed as a sum of terms for point charges centered on the atoms. The van der Waals interactions V_{vdW} are described by the Lennard-Jones (12–6) or the Buckingham potential (exp-6). When hydrogen bonding is present the Lennard-Jones (12–10) potential is sometimes used. General force fields such as AMBER, [37] AMBER/OPLS, [38] and DREIDING [39] can be used to accurately predict melting points for solids of compounds used in their parameterization. Based on the limited studies to date, it appears that for solids of fairly rigid molecules or ions, a general force field that has been parameterized to reproduce solid-state properties will predict the melting point within 10%. We have been interested in large nitro and nitramine compounds, e.g. 1,1-diamino-2,2-dinitroethylene (FOX-7), hexahydro-1,3,5-trinitro-1,3,5-*s*-triazine (RDX), and octahydro-1,3,5,7-tetranitro-1,3,5,7-tetraazacyclooctane (HMX). The structures of

Downloaded At: 17:57 14 January 2011

these molecules are shown in scheme 1. The molecules have active internal vibrational and torsional modes that allow conformational changes upon melting. These internal motions must be properly described by the force field for accurate simulations of melting. Furthermore, modifications are needed to describe the functional groups involving atom types not included in the parameterization of the standard force fields.

Socrescu, Rice, and Thompson (SRT) [40] have developed rigid-molecule force fields that accurately describe solid-state properties of most classes of energetic materials. In cases of flexible molecular structures, intramolecular bond stretching, angle bending, and torsional force field parameters were determined by electronic structure calculations. Molecular packing and *ab initio* MD calculations on the solid phases were used to determine intermolecular van der Waals parameters [41]. Electrostatic point charges used in the intermolecular potential have been determined by a variety of methods, including Mulliken analysis, [42] natural orbital analysis, [42] RESP, [43] and CHELPG [44]. The electronic polarizability of atoms may need to be taken into account to correctly reproduce some of the properties of some materials [45].

The SRT force fields [40] were originally developed assuming rigid molecules. Some studies have been done in which the SRT force fields were combined with intramolecular forces taken from AMBER, which show that modifications are required to correctly predict the density and melting point in some cases. Reparameterization is required to reproduce the solid density because the SRT was formulated assuming rigid molecules and thus when flexibility is introduced the resulting density is too small. This is illustrated by a study of dimethylnitramine (DMNA) using the AMBER force field combined with the SRT forces field [40(a)]. The SRT-AMBER force field predicts the solid-state properties in reasonable agreement with experimental results, but to predict the melting point to within 5% of the experimental value the HCNN and CNNO torsional barriers in the AMBER potential were replaced with values determined from *ab initio* electronic structure calculations. This is reasonable given that the AMBER force field is not parameterized for nitramines. Much of the validation of standard force fields has been done for particular states, i.e. solid, liquid or solution, but not for processes linking the states. More effort needs to be devoted to developing force fields that accurately treat the full range of materials (including hydrogen-bonded solids) for solid–liquid and solid–solid phase changes.

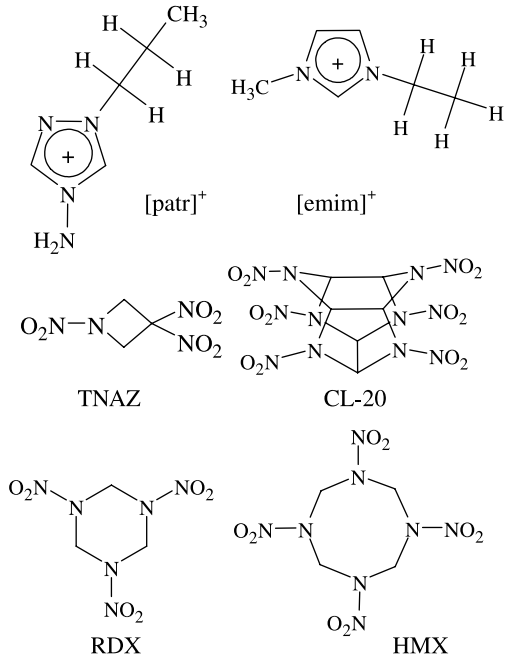

Scheme 1.

5. Brief reviews of selected studies

In this section we briefly review MD simulations of the melting of polyatomic molecular and ionic solids and nanoparticles. Most MD-based studies have been for atomic solids (Lennard-Jones and metals), thus the methods were mainly developed for atomic solids. Some modifications of the methods are required for applications to solids consisting of polyatomic molecules and ions, and some innovations are needed for computing melting points of nanoparticles. We offer here a very terse review of some applications of these methods. We do not attempt to be comprehensive, but rather focus on studies we have reported, studies that were carried out using DL_POLY. A basic motivation of the work we review was to determine the best methods for accurately simulating the melting of complex solids and nanoparticles for predicting thermodynamic melting points. An underlying impetus is to learn more about the atomic-level mechanisms by which melting occurs in various kinds of solids.

5.1 Molecular solids

The MD study of crystalline acetic acid by Gavezzotti [46] stands out as an early example of a simulation of melting of a polyatomic solid. Simulations of the NPT ensemble for the OPLS force field were carried out for the perfect crystal and for crystals with voids (6 out of 240 molecules were removed from the perfect crystal). The predicted melting point, with 2.5% voids, is in good agreement with the experimental value. The simulations predicted an amorphous state between the crystal and the melt, with little or no ordering of hydrogen bonding and only partial molecular mobility.

Solca *et al.* [17] and later Agrawal *et al.* [15(a)] investigated void-induced melting of argon. Agrawal *et al.* performed simulations using continuous heating. The results of their studies are consistent with previous work on the melting of Ar, [17] Ne, [17] and acetic acid [46]. The continuous heating was implemented as a modification in the dlpoly.f program in DL_POLY 2.15.

Downloaded At: 17:57 14 January 2011

After every 1000th time steps (0.5 ps) the temperature of the system was scaled from T to $T + \Delta T$, with $\Delta T = 10^{-4}$ K.

The introduction of voids in a simulation crystal is an ad hoc way of creating interfacial area to eliminate the free energy barrier to the formation of the solid–liquid interface that allows superheating in perfect crystals. Phillpot *et al.* [16] reported studies of various kinds of defects, including grain boundaries, free surfaces, and planar arrays of voids, in Cu and Solca *et al.* [17] performed some studies of void-induced melting in rare gas solids. These studies indicated that with the proper number of voids the predicted melting temperature could be taken to be the thermodynamic melting point. Agrawal *et al.* [15(a)] carried out systematic studies of the number and locations of voids in Ar crystals and found that the predicted melting point, which compares well with the experimental values, is independent of the location of the voids but, as found earlier by Solca *et al.* and others, is dependent on the number of voids with the agreement with experiment corresponding to simulations for the number of voids in the plateau region.

Agrawal *et al.* [15(b)] followed up their study of Ar with one to extend simulation methods to polyatomics. NM was simulated using incremental heating of crystals with voids. The effective heating rate was 2.0×10^{11} K/s. An order parameter for orthorhombic unit cells, the density, and energy per molecule were monitored as functions of the simulation time to determine the melting point. The RDF was calculated to confirm that melting had occurred. They also compared the results of simulations using the fully flexible force field of Sorescu *et al.* [47] and a rigid-molecule force field. The computed melting points using the two force fields differ by less than 3 K. As we will discuss below, that the intramolecular motions have little effect on the melting point is not generally the case but is due to the fact that NM has no vibrational modes that undergo large amplitude motions; i.e. it is not very floppy at the melting point temperature. Also, a two-phase solid–liquid NVE simulation was performed for comparisons with the void-induced melting simulations. The melting points obtained from the void-induced melting and two-phase simulations are 266.5 ± 7.7 and ~ 255.5 K, respectively. The experimental melting point of NM is 244.73 K.

An alternative calculation of NM melting using homogenous nucleation theory was reported by Zheng and Thompson [12]. They used equation (10) with a script to automatically set up consecutive DL_POLY runs at incrementally increasing temperatures, followed by equilibration steps. The heating rate of 8.9×10^9 K/s was employed in these calculations. The slower rate of heating in this calculation and better equilibration at each temperature leads to a calculated melting point of 251.1 K, which is in better agreement with the experimental value. These calculations also show that the bond lengths, angles and dihedral angles of NM are not significantly different before and after melting.

We note that even if the perfectly accurate force field were available one might expect an MD simulation using it (assuming the validity of classical mechanics) would predict a value for the melting point higher than the experimental value. Any imperfections or impurities in a sample in the laboratory would tend to lower the melting point. Thus, one should question a force field that predicts values lower than the measured melting point.

Zheng and Thompson [49] recently studied the predictions of three force fields on the calculated melting point of DMNA. The three force fields include the AMBER force field and two force fields custom designed for DMNA [40]. All three of the force fields give good predictions for solid-state properties of DMNA, but the AMBER force field gave the closest prediction to the experimental melting point of 331 K. By modifying the parameters for the torsional potential in the AMBER force field, a melting point of 346 K was calculated for DMNA, compared to 360 K for the unmodified AMBER force field. This study shows that the AMBER force field parameters are generally a good basis for calculating melting points of the nitramines. Similar studies for other classes of materials would be useful in determining the applicability of AMBER to other classes of materials.

The incremental heating void-induced melting method has also been used to determine the melting point of the more complex 1,3,3-trinitroazetidine (TNAZ, see scheme 1) [48] and RDX [49] solid phases. These materials are noteworthy because they are relatively flexible and some of their low-energy internal degrees of freedom are activated at temperatures near the melting point. It was observed for the RDX molecule that some of the dihedral angles undergo significant changes near the melting point. These modes can adsorb significant amounts of energy during the heating of the solid and if they are not properly described by the force field, the calculated melting point may differ considerably from the experimental value.

5.2 Ionic solids

We have investigated force fields and simulation methods to determine the reliability of the predictions of MD simulations of ionic solids. Room-temperature ionic liquids, which consist of various anions with organic cations, (RTILs) present interesting possibilities in a wide range of practical applications. The range of choices in the design of the structure of the cation provides the flexibility to design an RTIL with specific properties for specific applications. A critical property of an RTIL is its melting point, which can be manipulated by selection of the structures of the cation. A valuable theoretical tool for facilitating the design of novel RTILs would be a robust method for predicting melting points and other physical properties of a proposed new salt. Ammonium salts display interesting phase behavior as functions of temperature and pressure; we have studied the nitrate and dinitramide. These are excellent prototypical salts for

Downloaded At: 17:57 14 January 2011

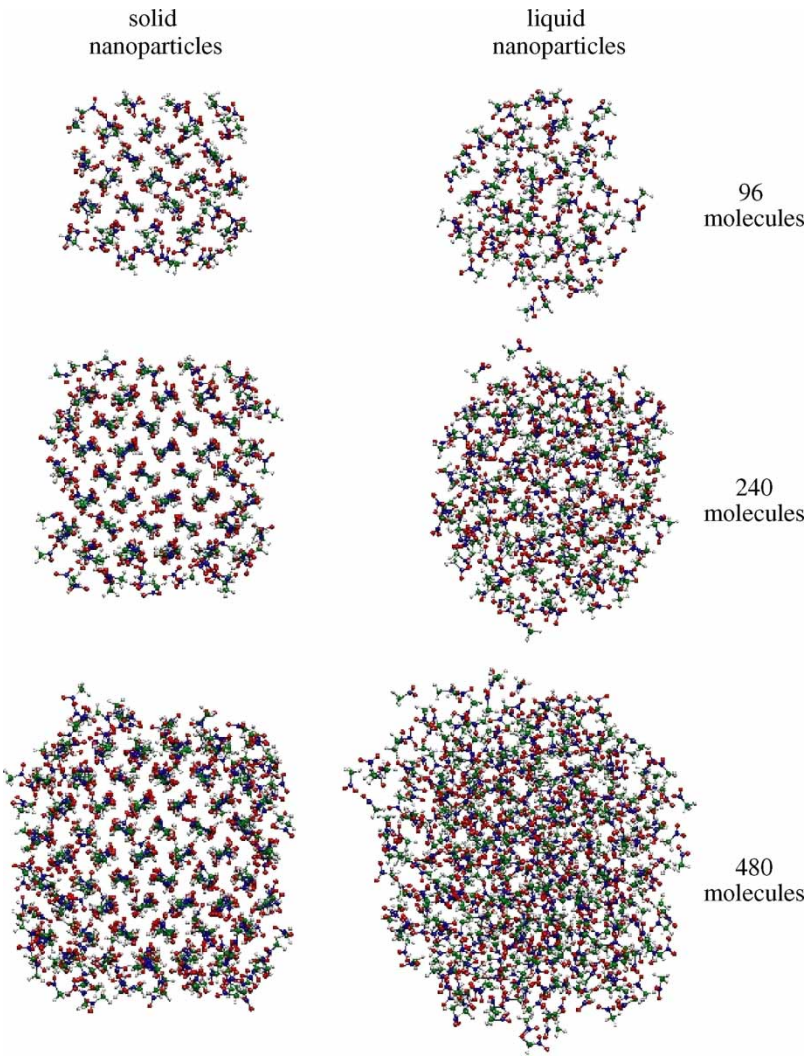

Figure 8. Snapshots of characteristic solid and liquid NM nanoparticles of various sizes. The initial configurations of the solid nanoparticles with 96, 240 and 480 molecules were taken from $4 \times 3 \times 2$, $5 \times 4 \times 3$ and $6 \times 5 \times 4$ repetitions of the unit cell of bulk solid NM.

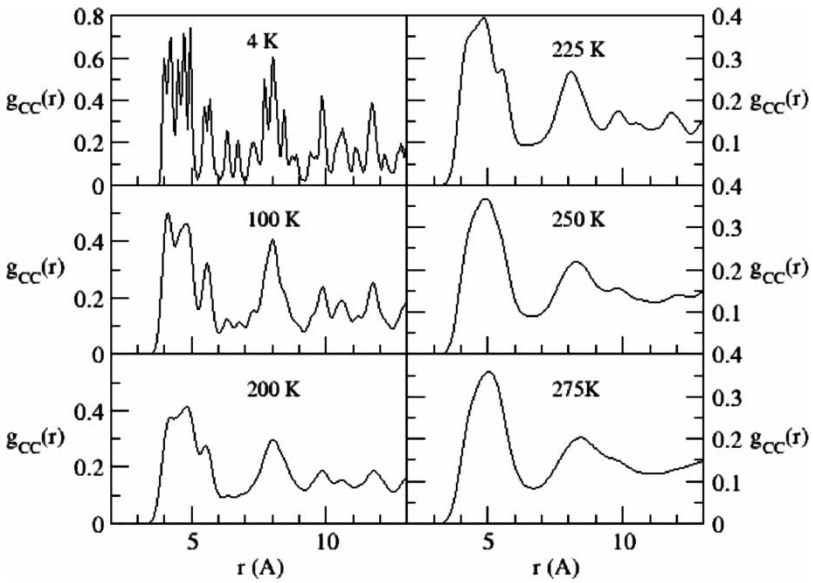

Figure 9. The carbon–carbon RDF for NM in the 480 molecule nanoparticle at six temperatures. Many of the long-range structural details in the RDF are lost upon melting of the nanoparticle. Short-range correlations and some long-range features due to dipole–dipole correlations are retained in the liquid nanoparticle. The melting range is between 220 and 240 K for this nanoparticle.

Downloaded At: 17:57 14 January 2011

Downloaded At: 17:57 14 January 2011

testing the feasibility of predicting complex behavior in ionic materials, particularly since there is reliable experimental data for validation of models and simulation methods in these two cases.

The melting point and solid- and liquid-state properties as functions of temperature and pressure of ammonium dinitramide (ADN), $NH_4N(NO_2)_2$, was calculated by Velardez *et al.* [50] using MD simulations. The intramolecular potential for ADN was obtained from the AMBER 7 program and the intermolecular potential from Sorescu and Thompson [41]. The simulations were performed for $3 \times 2 \times 4$, $5 \times 4 \times 6$ and $6 \times 4 \times 8$ supercells. The $3 \times 2 \times 4$ supercell is adequate for predicting the melting point; however, larger simulation cells had to be used to obtain converged results for the liquid-state properties. The melting point was determined by calculating the density, enthalpy, and RDF as functions of temperature. The temperature dependence of the diffusion coefficient, calculated using equilibrium time-correlation functions, shows a discontinuity at the melting temperature, and is a good indicator of the melting transition. The value of the normal melting temperature of the perfect crystal was calculated to be in the range 474–476 K; the measured values are in the range 365–368 K. The difference is mainly due to superheating of the perfect crystal. Simulations of crystals with eight or more voids predict a melting temperature in the range 366–368 K, which is in excellent agreement with experiment. Velardez *et al.* [50] also calculated the melting point for pressures up to 0.8 GPa, which is the highest experimental pressure for ADN reported by Russell *et al.* [51] The computed pressure dependence of the melting point is in excellent agreement with experimental results. This good agreement with experiment may be taken as preliminary evidence that force fields for ionic materials are more easily constructed because of the strong influence of the Coulombic interactions, which are easier to accurately determine than van der Waals interactions.

Velardez *et al.* [19(b)] have reported MD simulations using DL_POLY to study melting of ammonium nitrate (AN). Ammonium nitrate is known to exist at normal pressures in five crystal phases, usually labeled V, IV,..., I in order of increasing energy up to its melting point 442 K. The low-temperature phase V is an ordered structure with orthorhombic symmetry. There are two types of NO_3^- ions slightly distorted while the NH_4^+ ions are symmetrically equivalent. There are strong O...H hydrogen bonds in the solid phase. Sorescu and Thompson [52] developed a fully-flexible force field for AN-V. The intermolecular forces are described by a sum of Coulombic terms, Lennard-Jones 12–6 potentials, and 10–12 potentials (for the O...H hydrogen bonding interactions), and the intramolecular terms represented by the usual valence force field functions. Velardez *et al.* used this force field in MD simulations initiated with AN in phase II. Phase II has tetragonal symmetry with disorder due to equivalent alternative positions for both the ammonium and nitrate ions. Experiments show that at 357 K AN-II undergoes a transition to the highly disordered cubic phase I, which is the phase from which melting occurs.

Constant temperature and pressure (NPT) simulations were performed for a $4 \times 4 \times 5$ supercell of AN with voids over a wide range of temperatures and for atmospheric pressure. The thermodynamic melting point was predicted to be 445 ± 10 K, in excellent agreement with the experiment (442 K). A crystalline phase transition corresponding to II $\rightarrow$ I was observed prior to melting. The ammonium ions in phase II are rotationally free while the nitrate ions are not. The nitrate ions are arranged in parallel rows with planes that are perpendicularly oriented with respect to one another. The simulations showed that the nitrate ions retain their initial general orientations at 350 K, while undergoing librational motions about their equilibrium orientations; but are rotationally disordered at 400 K. Above 400 K both the ammonium and nitrate ions are essentially rotationally unhindered. The density and RDF show that this phase of AN is a solid.

Melting simulations have recently been reported for the RTILs ethyl-methylimidazolium hexafluorophostate [emim] [PF_6], [53] and 1-*n*-propyl-4-amino-1,2,4-triazolium bromide [patr] [Br] [13]. The structures of the cations of these salts are shown in scheme 1. The force fields were based on the one developed Canongia Lopes *et al.* [54] for imidazolium-based RTILs. The intermolecular force field parameters were taken from the AMBER/OPLS force field and the intramolecular parameters and electrostatic point charges were custom fit by Canongia Lopes *et al.* for this class of materials. We extended these force field parameters to the triazolium ionic liquid [patr] [Br]. Starting from the X-ray crystal structures, the predicted melting point for the [emim] [PF_6] is 375 ± 10 K which is approximately 13% larger than the experimental value of 333 K. For [patr] [Br] the calculated melting point is 360 ± 10 K, which is about 8% higher than the experimental value of 333 K. These agreements are achieved with no adjustments of the parameters in the AMBER/OPLS force field. Given the fact that the substituted triazolium cation has atom types that do not correspond to those given in the AMBER force field, this agreement is further evidence that the forces in ionic solids are easier to determine than in van der Waals solids. Or, in other words, the properties are less sensitive to the details of the interactions; exceptions may be ionic solids with large, floppy, organic cations. As the size of the organic cation of a RTIL increases the properties approach those of the organic solid.

It was observed in the [emim] [PF_6] [53] and [patr] [Br] [13] simulations that for a perfect crystal the superheating temperatures are higher than the normal 1.2 times the melting point. This could be due to the long side chains in the cation or strong intermolecular interactions in this ionic solid. In this case, the melting point prediction based on equation (10) is no longer valid.

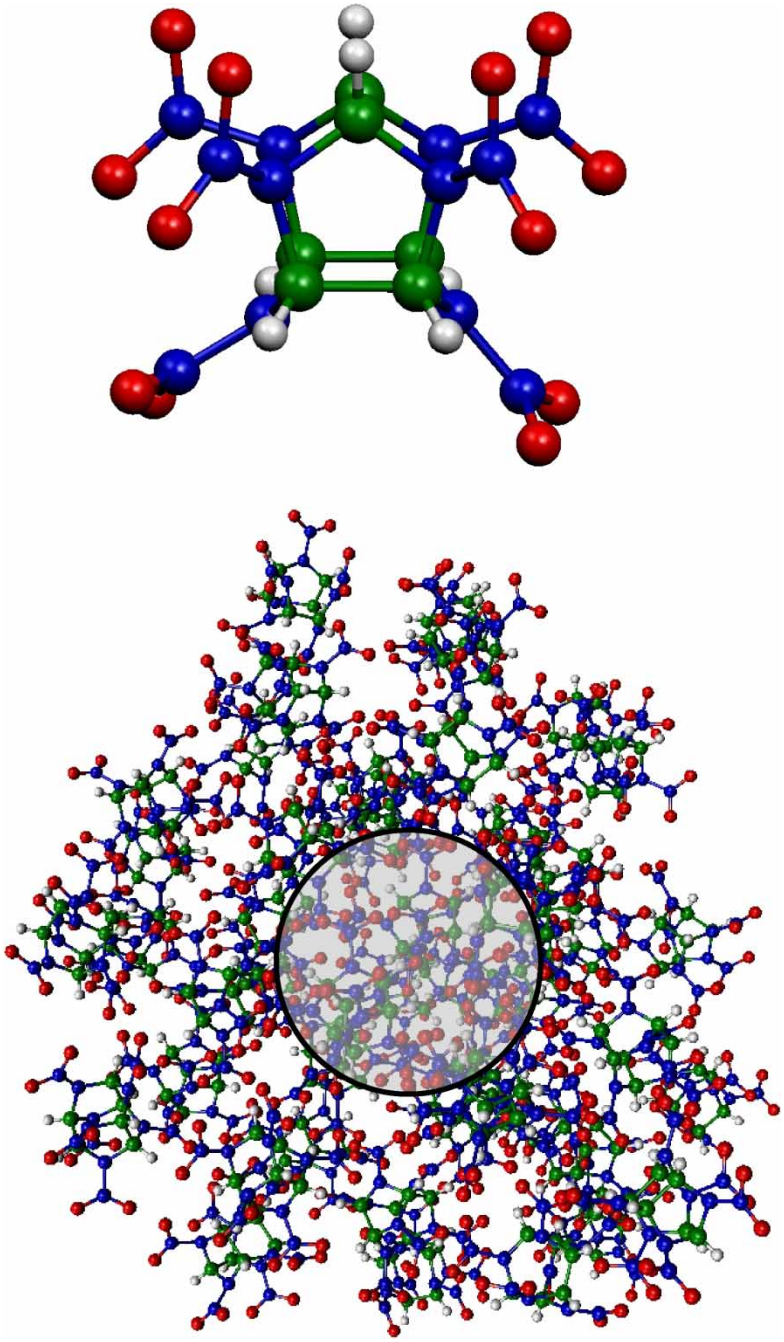

Figure 10. The structure of the CL-20 molecule and the 88 molecule CL-20 nanoparticle. A sphere is drawn, centered at the center-of-mass of the nanoparticle. The density of the nanoparticle can be estimated by determining the mass inside this sphere. This density can be useful for determining the melting point of the nanoparticle.

5.3 Nanoparticles

The melting of metallic nanoparticles has been extensively studied. Various tight-binding, imbedded-atom method, and simple pairwise additive potentials have been used in these studies. Here, we only discuss the MD studies of melting of the nanoparticles of the molecular materials NM [34] and 2,4,6,8,10,12-hexanitrohexaazaisowurtzitane (HNIW or CL-20, see scheme 1) [55].

Solid and liquid configurations of NM nanoparticles with 96, 240 and 480 molecules are shown in figure 8. These three nanoparticles were constructed by annealing from $4 \times 3 \times 2$, $5 \times 4 \times 3$ and $6 \times 5 \times 4$ replicas of the solid NM unit cell. The annealed solid nanoparticles are comprised of a reconstructed outer surface and a solid-like core, which retains some of the characteristics of the initial bulk structure. The liquid nanoparticles are roughly spherical in shape.

The melting points of nanoparticles of NM and CL-20 were characterized by the variation of the intermolecular energy, RDF, or diffusion coefficient with temperature. The carbon–carbon RDFs of the NM with 480 molecules at temperatures in the solid and liquid range are shown in figure 9. For solid nanoparticles, the RDF shows some

Downloaded At: 17:57 14 January 2011

Downloaded At: 17:57 14 January 2011

long-range structure, which is destroyed upon melting. The RDFs for $T = 250\,\mathrm{K}$ and higher show that the nanoparticle has melted. The dipole–dipole correlation function, equation (13), was also found to be useful for this purpose. The volume and density of a nanoparticle are not well-defined quantities but a heuristic procedure can be used to define a volume for a nanoparticle and check its variation with temperature. Spheres of different radii, r, are centered on the center of mass of the nanoparticle and the number of molecules within each sphere counted to determine the density of the nanoparticle in that sphere. A sample of such a sphere is shown superimposed on a nanoparticle of CL-20 in figure 10. Plotting the densities defined in this manner as a function of the sampling-sphere radius gives a fairly well converged density for the nanoparticle, which begins to decay as the spheres reach the surface of the nanoparticle. The nanoparticle density decays as $1/r^3$ as the measuring spheres encompass the outer boundaries of the nanoparticle. Just as the density of bulk solids decreases in a discontinuous manner, the density of nanoparticles (as defined above) also decreases discontinuously at the melting point; see figure 11 which shows the variation of the density of NM nanoparticles as a function of temperature. This decrease in density can be used to characterize the melting point of the nanoparticle. Unlike bulk solids for which the density and intermolecular energy of the phase changes abruptly at the melting point, for the NM nanoparticle it was observed that these quantities change over a range of temperatures. This behavior is seen in figure 11, which shows the density of the 96-, 144- and 240-molecule nanoparticles. This implies that in the nanoparticles the solid and liquid phases are in equilibrium over a range of temperatures that decreases with increasing particle size. The behavior of large nanoparticles (with 480 molecules) approaches that of the bulk solid phase; there is an abrupt density drop at the melting point. As noted in the discussion following equation (2), for a nanoparticle the additional surface degree of freedom at the solid–liquid equilibrium can lead to a variety of melting behaviors such as surface melting or bistability of the solid and liquid phases. The quantitative characterization of the melting of complex molecular materials is an issue that needs to be further addressed in future work.

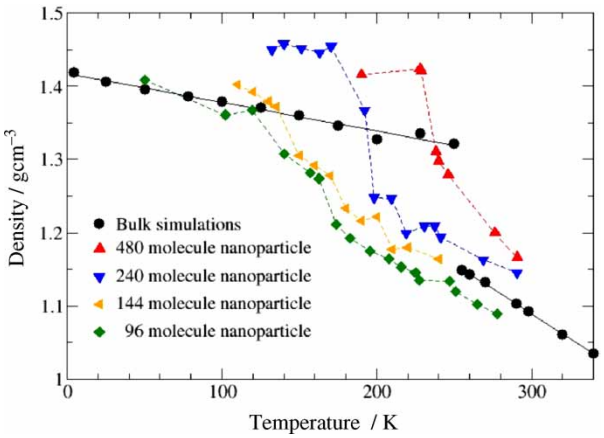

Figure 11. The variation of the density of nanoparticles of NM with temperature. The drop in the density shows the melting of the nanoparticle. For smaller nanoparticles, the density drop occurs over a broader range of temperature. This defines the solid–liquid equilibrium range for NM nanoparticles.

6. Conclusions

The melting points of a wide range of materials have been determined by MD simulations. These include rare gases, simple molecule solids, hydrogen-bonded complex molecular solids such as those of the nitramine energetic materials, simple binary ionic salts, and more complex ionic solids such as RTILs. For any material, the choice of the method used to calculate the melting point is determined by the size of the molecules of that material and the minimum size of the simulation cell require for the simulation method of choice. The methods have been reviewed and some applications that illustrate them have been described.

Methods for MD simulations of melting and the calculation of melting points have been reviewed. The thermodynamic melting point is defined by the equality of the free energies (chemical potentials) of the solid and liquid phase, and this can be used to compute the melting point with MD simulations. Also, the melting point can be determined in simulations corresponding to one of the actual melting mechanisms, namely, homogeneous nucleation melting, surface induced melting, or void (imperfection) induced melting. The free energy determination of the melting point is theoretically rigorous, but the other methods have been shown to have reasonable theoretical justifications, and they are easier to implement. These methods are complimentary and have been used to determine the melting points of a wide range of solids. Void-induced melting simulations allow a straightforward use of periodic boundary conditions at different pressures in NPT simulations and avoids problems associated with superheating. The simulations are straightforward to set up and require between 100 and 200 molecular or ion pairs to obtain converged results. More than 800 molecules can be required for a two-phase NVE solid–liquid simulation.

For molecular and ionic salts composed of small, relatively rigid molecules and ions, potential energy functions determined to reproduce solid- or liquid-state properties (far from the phase transition) appear to predict accurate melting points. Also, standard force fields such as AMBER have also been shown to reproduce the melting point with good accuracy for these kinds of solids. For large floppy molecules with internal degrees of freedom active at temperatures near the melting point, it is much more critical that the force field accurately describe the active internal modes; quantum chemistry calculations of isolated molecules have proven useful in determining the force constants and barrier to internal rotations.

Acknowledgements

We would like to thank our colleagues Drs P. M. Agrawal, B. M. Rice, D. C. Sorescu, G. F. Velardez, L. Zheng and A. Siavosh-Haghighi who have contributed to various aspects of the work discussed in this article. DLT is grateful the Army Research Office and the Air Force Office of Scientific Research for financial support.

References

[1] W. Smith, T.R. Forester, I.T. Todorov, M. Leslie (Eds.). DLPOLY 2.16, CCLRC. , Daresbury Laboratory, Cheshire, UK, 2006; I.T. Todorov, W. Smith, editors, DLPOLY 3.06, CCLRC, Daresbury Laboratory, Cheshire, UK, 2006. See: http://www.cse.clrc.ac.uk/msi/software/DL_POLY/index.shtml.

[2] D. Frenkel, B. Smit. *Understanding Molecular Simulation*, Academic Press, San Diego (2000).

[3] J.G. Kirkwood. Statistical mechanics of fluid mixtures. *J. Chem. Phys.*, **3**, 300 (1935).

[4] D. Frenkel, A.J.C. Ladd. New Monte Carlo method to compute the free energy of arbitrary solids. Application to the fcc and hcp phases of hard spheres. *J. Chem. Phys.*, **81**, 3188 (1984); E.J. Meijer, D. Frenkel, R.A. LeSar, A.J.C. Ladd. J. Chem. Phys. 92, 7570 (1990); J. Anwar, D. Frenkel, M.G. Noro. Calculation of the melting point of NaCl by molecular simulation. J. Chem. Phys. 118, 728 (2003).

[5] J.H. Rose, J.R. Smith, F. Guinea, J. Ferrante. Universal features of the equation of state for metals. *Phys. Rev. B*, **29**, 2963 (1984).

[6] G. Parsafar, E.A. Mason. Universal equation of state for compressed solids. *Phys. Rev. B*, **49**, 3049 (1994).

[7] B. Guillot, Y. Guissani. Chemical reactivity and phase behaviour of NH4Cl by molecular dynamics simulations. I solid–solid and solid–liquid equilibria. *J. Chem. Phys.*, **116**, 2047 (2002).

[8] G. Grochola. Constrained fluid λ-integration: Constructing a reversible thermodynamic path between the solid and liquid state. *J. Chem. Phys.*, **120**, 2122 (2004).

[9] D.M. Eike, J.F. Brennecke, E.J. Maginn. Toward a robust and general molecular simulation method for computing solid–liquid coexistence. *J. Chem. Phys.*, **122**, 014115 (2005).

[10] D.M. Eike, E.J. Maginn. Atomistic simulation of solid–liquid coexistence for molecular systems: Application to triazole and benzene. *J. Chem. Phys.*, **124**, 164503 (2006).

[11] S.-N. Luo, T.J. Ahrens. Superheating systematics of crystalline solids. *Appl. Phys. Lett.*, **82**, 1836 (2003); S.-N. Luo, T.J. Ahrens, T. Çağin, A. Strachan, W.A. Goddard III, D.C. Swift. Maximum superheating and undercooling: Systematics, molecular dynamics simulations, and dynamics experiments. Phys. Rev. B 68, 134206-1 (2003); (c) S.-N. Luo, A. Strachan, D.C. Swift. Nonequilibrium melting and crystallization of a model Lennard-Jones system. J. Chem. Phys. 120, 11640 (2004).

[12] L. Zheng, S.N. Luo, D.L. Thompson. Molecular dynamics of melting and the glass transition of nitromethane. *J. Chem. Phys.*, **124**, 154504 (2006).

[13] S. Alavi, D.L. Thompson. Simulations of the Solid, Liquid, and Melting of 1-*n*-Butyl-4-amino-1,2,4-triazolium Bromide. *J. Phys. Chem.*, **109**, 18127 (2005).

[14] J.R. Morris, C.Z. Wang, K.M. Ho, C.T. Chan. *Phys. Rev. B*, **49**, 3109 (1994); J.R. Morris, X. Song. The melting lines of model systems calculated from coexistence simulations. J. Chem. Phys. **116**, 9352 (2002); (c) S. Yoo, X.C. Zeng, J.R. Morris. The melting lines of model silicon calculated from coexisting solid–liquid lines. J. Chem. Phys. 120, 1654 (2004).

[15] P.M. Agrawal, B.M. Rice, D.L. Thompson. Molecular dynamics study of the effects of voids and pressure in defect-nucleated melting simulations. *J. Chem. Phys.*, **118**, 9680 (2003); P.M. Agrawal, B.M. Rice, D.L. Thompson. Molecular dynamics study of the melting of nitromethane. J. Chem. Phys. **119**, 9617 (2003).

[16] S.R. Phillpot, J.F. Lutsko, D. Wolf, S. Yip. Molecular-dynamics study of lattice-defect-nucleated melting in silicon. *Phys. Rev. B*, **40**, 2831 (1989); J.F. Lutsko, D. Wolf, S.R. Phillpot, S. Yip. Molecular-dynamics study of lattice-defect-nucleated melting in metals using an embedded-atom-method potential. Phys. Rev. B **40**, 2841 (1989).

[17] J. Solca, A.J. Dyson, G. Steinebrunner, B. Kirchner, H. Huber. Melting curve for argon calculated from pure theory. *Chem. Phys.*, **224**, 253 (1997); J. Solca, A.J. Dyson, G. Steinebrunner, B. Kirchner, H. Huber. Melting curve for neon calculated from pure theory. J. Chem. Phys. **108**, 4107 (1998).

[18] C. Kittel. *Introduction to Solid State Physics*, 5th ed., p. 538, Wiley, New York (1976).

[19] G.F. Velardez, S. Alavi, D.L. Thompson. Molecular dynamics studies of melting and liquid-state properties of ammonium dinitramide. *J. Chem. Phys.*, **119**, 6698 (2003); G.F. Velardez, S. Alavi, D.L. Thompson. Molecular dynamics studies of melting and solid-state transitions of ammonium nitrate. J. Chem. Phys. **120**, 9151 (2004).

[20] K. Lu, Y. Li. Homogeneous nucleation catastrophe as a kinetic stability limit for superheated crystal. *Phys. Rev. Lett.*, **80**, 4474 (1998); Z.H. Jin, P. Gumbsch, K. Lu, E. Ma. Melting mechanisms at the limit of superheating. Phys. Rev. Lett. **87**, 0557031 (2001).

[21] L. Zhang, Z.H. Jin, L.H. Zhang, M.L. Sui, K. Lu. Superheating of confined Pb thin films. *Phys. Rev. Lett.*, **85**, 1484 (2000).

[22] A. Proykova, R.S. Berry. Analogues in clusters of second-order transitions. *Z. Phys. D*, **40**, 215 (1997).

[23] K.-J. Hanszen. Theoretische Untersuchungen über den Schmelzpunkt kleiner Klügelchen. Ein Beitrag zur Thermodynamik der Grenzflächen. *Z. Phys.*, **157**, 523 (1960).

[24] S.L. Lai, J.Y. Guo, V. Petrova, G. Ramanath, L.H. Allen. Size-dependent melting properties of small tin particles: Nanocalorimetric measurements. *Phys. Rev. Lett.*, **77**, 99 (1996).

[25] C.R.M. Wronski. The size dependence of the melting point of small particles of tin. *Br. J. Appl. Phys.*, **18**, 1731 (1967).

[26] V.P. Skiprov, V.A. Koverda, V.N. Skokov. Size effect on melting of small particles. *Phys. Status Solidi A*, **66**, 109 (1981).

[27] F.G. Shi. Size dependent thermal vibrations and melting in nanocrystals. *J. Mater. Res.*, **9**, 1307 (1994).

[28] B.R. Laird, R.L. Davidchack. Direct calculation of the crystal-melt interfacial free energy via molecular dynamics computer simulation. *J. Phys. Chem. B*, **109**, 17802 (2005).

[29] X.-M. Bai, M. Li. Calculation of solid–liquid interfacial free energy: A classical nucleation theory based approach. *J. Chem. Phys.*, **124**, 124707 (2006).

[30] T.L. Beck, J. Jellinek, R.S. Berry. Rare gas clusters: Solids, liquids, slush, and magic numbers. *J. Chem. Phys.*, **87**, 545 (1987); R. Kunz, R.S. Berry. Multiple phase coexistence in finite systems. Phys. Rev. E **49**, 1895 (1994); D.J. Wales, R.S. Berry. Coexistence in finite systems. Phys. Rev. Lett. **73**, 2875 (1994); K.D. Ball, R.S. Berry, R.E. Kunz, F.-Y. Li, A. Proykova, D.J. Wales. From topologies to dynamics on multidimensional potential energy surfaces of atomic clusters. Science **271**, 963 (1996).

[31] P. Noziéres, L. Verlet. Computer "experiments" on classical fluids. I. thermodynamical properties of Lennard-Jones molecules. *Phys. Rev.*, **159**, 98 (1967).

[32] M.P. Allen, D.J. Tildesley. *Computer Simulation of Liquids*, Oxford, Oxford (2000).

[33] J.M. Haile. *Molecular Dynamics Simulation. Elementary Methods*, Wiley, New York (1992).

[34] S. Alavi, D.L. Thompson. A molecular dynamics study of structural and physical properties of nitromethane nanoparticles. *J. Chem. Phys.*, **120**, 10231 (2004).

[35] S. Alavi, D.L. Thompson. Molecular dynamics simulations of the melting of aluminum nanoparticles. *J. Phys. Chem. A*, **110**, 1518 (2006).

[36] R.S. Berry, J. Jellinek, G. Natanson. Melting of clusters and melting. *Phys. Rev. A*, **30**, 919 (1984); Y.J. Lee, E.-K. Lee, S.Kim, R.M. Nieminen. Effect of the potential energy distribution on the melting of clusters. Phys. Rev. Lett. **86**, 999 (2001); Y. Zhou, M. Karplus, K.D. Ball, R. S.Berry. The distance fluctuation criterion for melting: Comparison of square-well and Morse potential models for clusters and homopolymers. J. Chem. Phys. **116**, 2323 (2002); J. Westergren, S. Nordholm, A. Rośen.Melting of palladium clusters – Canonical and microcanonical Monte Carlo simulation. Phys. Chem. Chem. Phys. **5**, 136 (2003).

[37] W.D. Cornell, P. Cieplak, C.L. Bayly, I.R. Gould, K.M. Merz Jr, D.M. Ferguson, D.C. Spellmeyer, T. Fox, J.W. Caldwell, P.A. Kollman. A second generation force field for the simulation of

Downloaded At: 17:57 14 January 2011

proteins, nucleic acids, and organic molecules. *J. Am. Chem. Soc.*, **117**, 5179 (1995) See also, http://amber.scripps.edu.

[38] W.L. Jorgensen, D.S. Maxwell, J. Tirado-Rives. Development and testing of the OPLS All-atom force field on conformational energetics and properties of organic liquids. *J. Am. Chem. Soc.*, **118**, 11225 (1996).

[39] S.L. Mayo, B.D. Olafson, W.A. Goddard III. DREIDING: A generic force field for molecular simulations. *J. Phys. Chem.*, **94**, 8897 (1990).

[40] D.C. Sorescu, B.M. Rice, D.L. Thompson. Intermolecular potential for the hexahydro-1,3,5-s-triazine Crystal (RDX): A crystal packing, Monte Carlo, and molecular dynamics study. *J. Phys. Chem. B*, **101**, 798 (1997); D.C. Sorescu, B.M. Rice, D.L. Thompson. Molecular packing and NPT-molecular dynamics investigation of the transferability of the RDX intermolecular potential to 2,4,6,8,10,12-hexanitrohexaazaisowurtizitane. J. Phys. Chem. B **102**, 948 (1998); D.C. Sorescu, B.M. Rice, D.L. Thompson. A transferable intermolecular potential for nitramine crystals. J. Phys. Chem. A **102**, 8383 (1998); D.C. Sorescu, B.M. Rice, D.L. Thompson. Molecular packing and molecular dynamics study of the transferability of a generalized nitramine intermolecular potential to non-nitramine crystals. J. Phys. Chem. A **103**, 989 (1999).

[41] D.C. Sorescu, L. Thompson. Classical and quantum mechanical studies of crystalline ammonium dinitramide. *J. Phys. Chem. B*, **103**, 6774 (1999).

[42] I.R. Levine. *Quantum Chemistry*, 4th ed., Prentice Hall, Englewood Cliffs, NJ (1991).

[43] C. Bayly, P. Cieplak, W. Cornell, P.A. Kollman. A well-behaved electrostatic potential based method using charge restraints for deriving atomic charges: the RESP model. *J. Phys. Chem.*, **97**, 10269 (1993).

[44] C.M. Breneman, K.B. Wiberg. Determining atom-centered monopoles from molecular electrostatic potentials. The need for high sampling density in formamide conformational analysis. *J. Comp. Chem.*, **11**, 361 (1990).

[45] T. Yan, C.J. Burnham, M.G. Del Pópolo, G.A. Voth. Molecular dynamics simulation of ionic liquids: The effect of electronic polarizability. *J. Phys. Chem. B*, **108**, 11877 (2004).

[46] A. Gavezzotti. A molecular dynamics view of some kinetic and structural aspects of melting in the acetic acid crystal. *J. Mol. Struct.*, **485–486**, 485 (1999).

[47] D.C. Sorescu, B.M. Rice, D.L. Thompson. Theoretical studies of solid nitromethane. *J. Phys. Chem. B*, **104**, 8406 (2000).

[48] P.M. Agrawal, B.M. Rice, L. Zheng, G.F. Velardez, D.L. Thompson. Molecular dynamics simulations of the melting of 1,3,3-trinitroazetidine. *J. Phys. Chem. B*, **110**, 5721 (2006).

[49] L. Zheng, D.L. Thompson. Molecular dynamics simulations of the melting of hexahydro-1,3,5-trinitro-1,3,5-*s*-triazine (RDX). *J. Chem. Phys.*, Submitted for publication.

[50] G.F. Velardez, S. Alavi, L. Thompson. Molecular dynamics studies of melting and liquid properties of ammonium dinitramide. *J. Chem. Phys.*, **119**, 6698 (2003).

[51] T.P. Russell, G.J. Piermarini, S. Block, J. Miller. Pressure, temperature reaction phase diagram for ammonium dinitramide. *J. Phys. Chem. B*, **100**, 3248 (1996).

[52] D.C. Sorescu, D.L. Thompson. Classical and quantum mechanical studies of crystalline ammonium nitrate. *J. Phys. Chem. A*, **105**, 724 (2001).

[53] S. Alavi, D.L. Thompson. Molecular dynamics studies of melting and some liquid-state properties of 1-ethyl-3-methylimidazolium hexafluorophosphate [emim] [PF6]. *J. Chem. Phys.*, **122**, 154704 (2005).

[54] J.N. Canongia Lopes, J. Deschamp, A.A.H. Pádua. Modeling ionic liquids using a systematic all-atom force field. *J. Phys. Chem. B*, **108**, 2038 (2004); J.N. Canongia Lopes, J. Deschamp, A.A.H. Pádua. Erratum J. Phys. Chem. B **108**, 11250 (2004).

[55] S. Alavi, G.F. Velardez, D.L. Thompson. Molecular dynamics studies of nanoparticles of energetic materials. *Mat. Res. Soc. Symp. Proc.*, **800**, 329 (2004).

Downloaded At: 17:57 14 January 2011